Prepared for submission to JCAP

A realistic assessment of the CTA sensitivity to dark matter annihilation

Hamish Silverwood,[a] **Christoph Weniger,**[a] **Pat Scott**[b] **and Gianfranco Bertone**[a]

[a]GRAPPA, University of Amsterdam
Science Park 904, 1098 XH Amsterdam, The Netherlands
[b]Department of Physics, Imperial College London,
Blackett Laboratory, Prince Consort Road, London SW7 2AZ, United Kingdom

E-mail: h.g.m.silverwood@uva.nl, c.weniger@uva.nl, p.scott@imperial.ac.uk, gf.bertone@gmail.com

Abstract. We estimate the sensitivity of the upcoming CTA gamma-ray telescope to DM annihilation at the Galactic centre, improving on previous analyses in a number of significant ways. First, we perform a detailed analyses of all backgrounds, including diffuse astrophysical emission for the first time in a study of this type. Second, we present a statistical framework for including systematic errors and estimate the consequent degradation in sensitivity. These errors may come from *e.g.* event reconstruction, Monte Carlo determination of the effective area or uncertainty in atmospheric conditions. Third, we show that performing the analysis on a set of suitably optimised regions of interest makes it possible to partially compensate for the degradation in sensitivity caused by systematics and diffuse emission. To probe dark matter with the canonical thermal annihilation cross-section, CTA systematics like non-uniform variations in acceptance over a single field of view must be kept below the 0.3% level, unless the dark matter density rises more steeply in the centre of the Galaxy than predicted by a typical Navarro-Frenk-White or Einasto profile. For a contracted $r^{-1.3}$ profile, and systematics at the 1% level, CTA can probe annihilation to $b\bar{b}$ at the canonical thermal level for dark matter masses between 100 GeV and 10 TeV.

arXiv:1408.4131v1 [astro-ph.HE] 18 Aug 2014

Contents

1 Introduction **1**

2 The CTA and *Fermi*-LAT experiments **2**
2.1 The CTA and other imaging air Cherenkov telescopes 2
2.2 The Fermi Large Area Telescope 5

3 The dark matter signal **5**

4 Backgrounds **6**
4.1 Cosmic-ray background 6
4.2 Diffuse gamma-ray background 8

5 Analysis **9**
5.1 Analysis regions and J factors 9
5.2 Statistical framework 9
5.3 Background treatment 11

6 Results **11**
6.1 Point source sensitivity 12
6.2 Galactic centre sensitivity with Ring method 13
6.3 Galactic centre sensitivity with multi-bin morphological method 14
6.4 Projected cross-section limits 16

7 Conclusion **19**

1 Introduction

Current and upcoming gamma-ray experiments are ideally suited to probing the nature of dark matter (DM), by searching for high-energy photons from annihilation of Weakly Interacting Massive Particles (WIMPs; [1–5]). Other so-called *indirect* DM detection strategies include searches for neutrinos [6–11] or anti-matter [12–18] produced by DM annihilation. Indirect detection is particularly appealing at the present time, owing to a lack of convincing evidence from DM *direct* detection [19–24], which seeks to measure energy exchanged in collisions between nuclei and DM in underground experiments, and *collider* searches looking for new particles at the Large Hadron Collider [5, 25–28].

Recent data from the Large Area Telescope (LAT) aboard the *Fermi* satellite set stringent and robust limits on the annihilation cross section of WIMPs as a function of the DM particle mass, based on a lack of excess gamma-ray emission from dwarf spheroidal galaxies [29]. *Fermi* data have also led to the discovery of excess emission from the Galactic centre (GC), which has been interpreted in terms of DM annihilation (see *e.g.* Ref. [30] and references therein). Furthermore, the Imaging Air Cherenkov Telescopes (IACTs) HESS, VERITAS and MAGIC search for DM signals in dwarf spheroidal galaxies and the GC [31–33], with the current strongest limits on TeV-scale DM coming from HESS observations of the GC [34].

One of the next major steps in high-energy gamma-ray astrophysics will be the construction of the Cherenkov Telescope Array (CTA), which is currently in the design phase [35] and expected to start operations in 2019. Several estimates of the sensitivity of CTA to gamma-rays from DM annihilation exist in the literature. All of these agree on the fact that CTA will improve existing constraints for values of the DM particle mass above $\mathcal{O}(100)$ GeV, but substantial differences exist, up to one order of magnitude or more in annihilation cross section for a given mass, depending on the assumptions made about the telescope array configuration, analysis setup and observation time [36–38].

In this paper we carry out a new estimation of the sensitivity of CTA to DM annihilation, and compare this to the sensitivity of *Fermi*. We improve on previous analyses in a number of ways. First, we present a detailed discussion of all backgrounds, including cosmic-ray protons and electrons, and for the first time in the context of CTA and DM, the effects of the diffuse astrophysical emission. We estimate this from *Fermi*-LAT data, suitably extrapolated above 500 GeV in order to cover the range of energies relevant for CTA. Second, we study the impact of systematic errors. There are many sources of systematic uncertainty inherent in CTA measurements: event reconstruction, Monte Carlo determination of the effective area, and uncertainty in atmospheric conditions [35]. A detailed assessment can only realistically be performed by the CTA Collaboration itself after the instrument is built; here we instead present a simple but comprehensive statistical framework with which the impacts of these systematics on the sensitivity of CTA to DM annihilation can be illustrated and evaluated. Third, we show that performing the analysis over a series of suitably optimised regions of interest (RoIs) partially compensates for the degradation in sensitivity due to systematics and backgrounds. We carry out a multi-RoI 'morphological' analysis of the gamma-ray emission, and demonstrate how it improves the CTA sensitivity to DM compared to the so-called 'Ring' method previously discussed in the literature [36].

The paper is organised as follows: in Sec. 2 we describe the CTA and *Fermi*-LAT experiments; in Sec. 3 we review the basics of indirect detection with gamma-rays; in Sec. 4 we discuss and quantify the cosmic-ray and diffuse gamma-ray background for CTA; in Sec. 5 we present our analysis strategy, in particular the implementation of systematic errors and the RoIs relevant for our analysis; we present our results in Sec. 6 and conclusions in Sec. 7.

2 The CTA and *Fermi*-LAT experiments

2.1 The CTA and other imaging air Cherenkov telescopes

Gamma rays in the GeV to TeV regime initiate electromagnetic cascades in the atmosphere, which start at an altitude of 10–20 km and generate a focused cone of Cherenkov light that typically covers several hundred meters on the ground. Air Cherenkov telescopes detect gamma rays by observing this dim Cherenkov light with optical telescopes. The overall light yield, the shape and the orientation of the air shower gives information about the energy and arrival direction of the gamma ray. Because observations can only be performed during (nearly) moonless nights, the observation time per year is limited to approximately 1000 hours.

Current active Imaging Air Cherenkov Telescopes (IACTs) are HESS II (Namibia; [39]), VERITAS (Arizona; [40]), and MAGIC (La Palma[1]). Although all three instruments have an active program to search for DM signals in various regions of the sky (see *e.g.* Refs. [31–33]),

[1] http://magic.mpp.mpg.de/

only HESS can observe the GC high above the horizon ($\theta_z \sim 6^\circ$, compared to $\theta_z \gtrsim 57^\circ$ for VERITAS and MAGIC). As a shorter transmission length through the atmosphere allows for a lower threshold energy, HESS is ideally situated to search for DM signals from the GC. Non-detection of a DM signal by HESS provides the strongest current limits on the DM self-annihilation cross section, for DM masses around the TeV scale [34].

CTA will consist of several tens of telescopes of 2–3 different types, with sizes between about 5 and 24 meters, covering an area of several square kilometres. The sensitivity will be a factor ten better than current instruments, the field of view (FoV) will be up to 10° in diameter, and the energy threshold $\mathcal{O}(10\,\mathrm{GeV})$.

CTA is envisaged as a two-part telescope, with southern and northern sites. CTA South is the most relevant for DM searches towards the Galactic centre. The location of the southern array has not yet been settled, but the main candidates are now the Khomas Highlands in Namibia and Cerro Paranal in Chile. The final design is also not yet fixed. Apart from construction and maintenance questions, relevant remaining design choices are the relative emphasis on higher or lower energies, the angular and energy resolution, and the FoV. A first detailed Monte Carlo (MC) analysis was presented in Ref. [41], where 11 different configurations for the southern array were discussed. Depending on the array configuration and gamma-ray energy, the point source sensitivity varies within a factor of five,[2] and can be further improved by about a factor of two with alternative analysis methods [41].

In this paper we will concentrate on the proposed configuration known as 'Array I' [41],[3] which is a balanced configuration with three large (∼24 m aperture), 18 medium (∼12 m) and 56 small telescopes (∼4–7 m). This configuration provides a good compromise in sensitivity between low and high energies. One advantage of using Array I is that extensive information on the effective area, angular resolution, energy resolution and background rates is available. Furthermore, a very similar array has been used in previous DM sensitivity studies: Array E in Ref. [36], and the Paris-MVA version of Array I in Ref. [38]. The point-source sensitivities of Arrays E and I agree very well at energies $\lesssim 1\,\mathrm{TeV}$, whereas at higher energies Array I is more sensitive (but only by a factor of less than two).

For convenience, here we summarise some of the main performance aspects of Array I: it features an effective area of about $100\,\mathrm{m}^2$ at its threshold energy of 20 GeV, which then increases quickly with energy to about $4 \times 10^5\,\mathrm{m}^2$ at 1 TeV and $3 \times 10^6\,\mathrm{m}^2$ at 10 TeV. The angular resolution in terms of the 68% containment radius is about $r_{68} \simeq 0.3^\circ$ at threshold, and drops to below 0.06° at energies above 1 TeV. The energy resolution is relatively large at threshold, with $\sigma(E)/E \simeq 50\%$, but drops to below 10% at energies above 1 TeV.

As we will discuss below in more detail, the large effective area, irreducible background of cosmic-ray (CR) electrons, and the fact that electrons look identical to photons for an IACT, mean that the number of events passing analysis cuts will be extremely high, especially at low energies and for analyses of diffuse and extended sources. Statistical errors will therefore be small, making systematic uncertainties in the event identification particularly important. In fact, in the case of searches for DM particles with GeV to TeV masses, these systematics will turn out to be one of the limiting factors. Detailed instrumental uncertainties (*e.g.* the covariance matrix of reconstruction efficiencies in different regions of the FoV) will probably only become available once the instrument starts to operate, so in this paper we resort to a few well-motivated benchmark scenarios.

[2] This is based on the adoption of a standard Hillas-based analysis. This is a classical analysis method, based on zeroth (amplitude), first (position) and second (width and orientation) momenta of the images [42].

[3] In particular, we adopt the version based on the Hillas-parameter analysis of the MPIK group.

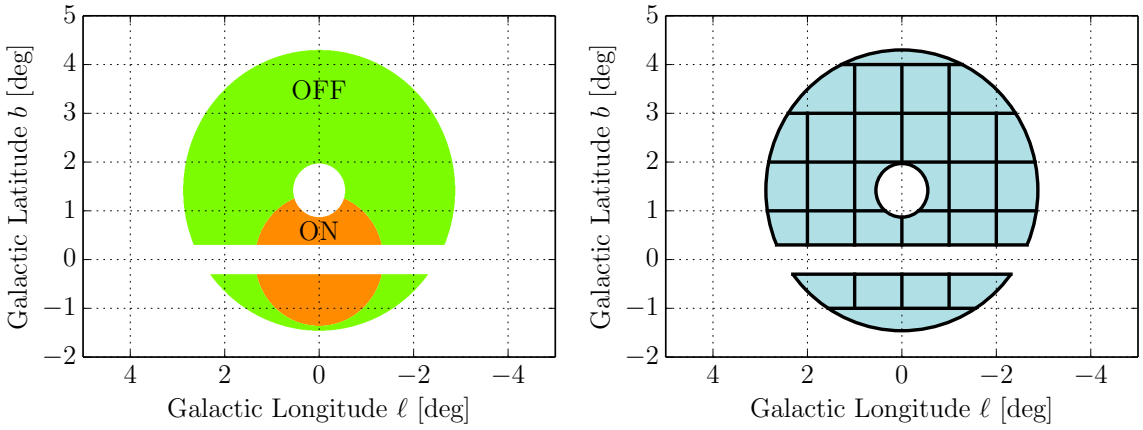

Figure 1. The different RoIs that we consider in this paper. *Left:* RoIs used in the Ring method of Ref. [36] as 'signal' and 'background' regions; we refer to these as simply 'ON' and 'OFF' regions, respectively. *Right:* Separation of the ON and OFF RoIs into 28 sub-RoIs, which we use in our morphological analysis.

The traditional observing strategy employed by IACTs in searching for DM annihilation (*e.g.* Ref. [34]) involves defining two regions on the sky expected to have approximately the same regular astrophysical emission, but different amounts of DM annihilation. The region with the larger expected annihilation is dubbed the 'ON' region, the other is called the 'OFF' region, and the analysis is performed using a test statistic defined as the difference in photon counts from the two regions. This is referred to as an 'ON-OFF' analysis, and obviously obtains the most power when the ON and OFF RoIs are chosen to differ as much as possible in their predicted annihilation rates.

The RoIs chosen for ON-OFF analyses may lie in the same or very different FoVs. Different FoVs allow a greater contrast in DM signal between ON and OFF regions, but have the potential to introduce differential systematics across the two FoVs. The 'Ring method' [36] is an ON-OFF analysis technique optimised for DM searches towards the GC with IACTs, which fits the ON and OFF regions into a single FoV, producing an approximately constant acceptance across the entire analysis region. Although both regions are expected to contain DM and background contributions, in the Ring method the ON and OFF regions are typically referred to as the 'signal' and 'background' regions. For simplicity, here we just call them ON and OFF.

A simple way to model the results of an ON-OFF analysis is to construct a Skellam likelihood [38, 43, 44], which is based on the expected difference between two Poisson counts (*i.e.* in the ON and OFF regions). However, once the assumption that astrophysical backgrounds are identical in the ON and OFF regions becomes questionable, a more straightforward method is simply to carry out a regular binned likelihood analysis. In this case, one predicts the photon counts in each RoI using detailed background and signal models, and compares them directly to the absolute number of photons observed in each RoI. This is the strategy that we investigate here for CTA, using both the original Ring method RoIs and a finer spatial binning. We show these two sets of RoIs in Fig. 1, and discuss their optimisation in Sec. 5. We still refer to the two-RoI analysis as the 'Ring method' even though we carry out a full likelihood analysis rather than an ON-OFF analysis. We refer to the multi-RoI analysis as

a 'morphological analysis', as it uses the expected spatial distribution of the DM signal to improve limits.

2.2 The Fermi Large Area Telescope

The LAT aboard the *Fermi* satellite is a pair-conversion detector, with a large FoV and an energy range from 30 MeV to above 300 GeV. Since its launch in 2008 the dominant observation strategy has been a full-sky survey providing roughly equal exposure in all directions of the sky. The *Fermi*-LAT is a formidable tool in the search for signals of DM annihilation. It currently provides the strongest constraints on the DM self-annihilation cross section, based on a combined observation of 15 dwarf spheroidal galaxies [29].

The *Fermi*-LAT provides an accurate measurement of the Galactic diffuse emission (GDE) up to energies of about 100 GeV. Above 100 GeV the number of detected photons becomes very small, due to the LAT's comparatively small effective area (~ 8000 cm^2). This is about the energy where the acceptance of IACTs starts to become sizable. Close to the Galactic disc and the GC, LAT measurements are actually dominated by GDE. This diffuse emission will be a critical foreground for any DM search, and—depending on the details of the search strategy—might mimic a DM signal.

Compared to IACTs, the LAT is an extremely clean gamma-ray telescope. Its plastic scintillator anti-coincidence detector, together with cuts on different event reconstruction quality estimators, allows proton and electron contamination in the gamma-ray sample to be suppressed to a level well below the very dim extragalactic gamma-ray background. The main uncertainties in the measured fluxes, especially at the high energies we are interested in, are hence of a statistical nature. The systematic uncertainty of the effective area is at the level of 10% [45], so we will neglect it throughout.

3 The dark matter signal

Assuming that the annihilation cross-section of DM does not depend on the relative velocity between particles, the calculation of the gamma-ray flux from DM annihilation can be divided into two parts.

The first part accounts for the DM distribution, and is commonly known as the 'J-factor'. This is an integral of the DM density squared along the lines of sight (l.o.s.) within a cone $\Delta\Omega$ that covers a certain RoI:

$$J\left(\Delta\Omega\right) = \int_{\Delta\Omega} \mathrm{d}\Omega \int_{\mathrm{l.o.s}} \mathrm{d}l\, \rho_{\mathrm{DM}}(r)^2. \tag{3.1}$$

The DM density profiles seen in N-body simulations of Milky-Way type galaxies are best fit by the Einasto profile [46]

$$\rho_{\mathrm{DM}}(r) \propto \exp\left(-\frac{2}{\alpha}\left[\left(\frac{r}{r_s}\right)^{\alpha} - 1\right]\right), \tag{3.2}$$

which we assume for our calculation of the J-factors for the GC. We normalise to a local DM density of $\rho_{\mathrm{DM}}(r_\odot) = 0.4\,\mathrm{GeV\,cm^{-3}}$, choosing $\alpha = 0.17$, $r_s = 20\,\mathrm{kpc}$, and $r_\odot = 8.5\,\mathrm{kpc}$ [47].

We will also use a slightly contracted generalised NFW profile, to indicate how limits would improve with a more optimistic DM distribution. We parameterise this profile as

$$\rho_{\mathrm{DM}}(r) \propto \frac{1}{r^{\gamma}(r_s + r)^{3-\gamma}}\,, \tag{3.3}$$

where $\gamma = 1.3$ is the inner slope of the profile that we will adopt below, and $r_s = 20\,\mathrm{kpc}$ the scale radius. We normalised this profile in the same way as the Einasto profile (Eq. 3.2).

The second part of the flux calculation covers the actual particle model for DM. Together with the J-factor, it yields the differential flux of DM signal photons,

$$\frac{\mathrm{d}\Phi}{\mathrm{d}E} = \frac{\langle\sigma v\rangle}{8\pi\, m_{\mathrm{DM}}^2} \frac{\mathrm{d}N_\gamma}{\mathrm{d}E}\, J\,(\Delta\Omega)\,. \tag{3.4}$$

Here $\langle\sigma v\rangle$ is the velocity-averaged DM self-annihilation cross section, in the limit of zero relative velocity. The DM mass is given by m_{DM}, and $\mathrm{d}N_\gamma/\mathrm{d}E$ is the annihilation spectrum, *i.e.* the average number of photons produced per annihilation per energy interval, which depends on the particular annihilation channel. For the gamma-ray yields, we will take the results from Ref. [48].

To calculate the expected number of signal events in a given observing time T_{obs}, between energies E_0 and E_1, we weight Eq. (3.4) by the energy-dependent effective area A_{eff} and integrate over the energy range in question,

$$\mu^{\mathrm{DM}} = T_{\mathrm{obs}} \int_{E_0}^{E_1} \mathrm{d}E\, \frac{\mathrm{d}\Phi}{\mathrm{d}E} A_{\mathrm{eff}}(E). \tag{3.5}$$

Note that for simplicity, throughout this paper we neglect the effects of the finite angular and energy resolution of CTA, as well as variations of the effective area within the FoV. As discussed above, the 68% containment radius of the point spread function (PSF) is around $\theta_{68\%} \simeq 0.3^\circ$ at the lowest energies that we consider, and significantly better at high energies. This is significantly smaller than the RoIs that we adopt (*cf.* Fig. 1). The energy resolution at 20 GeV is however quite large ($\sigma(E)/E \simeq 50\%$), and should be taken into account when interpreting the differential sensitivities that we quote below (Sec. 6). We checked that smearing a $b\bar{b}$ spectrum with a log-normal distribution with a width of $\sigma(\ln E)/\ln E = 50\%$ increases the peak signal flux relative to an assumed E^{-2} background by a factor of about 1.5; for $\sigma(\ln E)/\ln E = 20\%$ this drops to a factor of 1.1. This is mostly due to event migration from smaller to higher energies. Neglecting the finite energy resolution of CTA will hence affect our projected limits at most by a few tens of percent.[4]

4 Backgrounds

The dominant backgrounds for DM searches at the GC are the GDE and, in case of IACTs, the flux of cosmic rays that pass the photon cuts. Here we discuss the characteristics of these components, and describe how they enter our analysis.

4.1 Cosmic-ray background

CR electrons constitute an essentially irreducible background for gamma-ray observations with IACTs, because the electromagnetic cascades that they induce are practically indistinguishable from those caused by gamma rays. A possible way to discriminate between the two is to use the detection of Cherenkov light from the primary particle as a veto. This is however beyond the reach of current and next-generation instruments [35]. Due to their relatively soft spectrum, CR electrons are especially relevant at low energies, were they are

[4] For an analysis including the effects of energy resolution see Ref. [38].

responsible for most of the measured flux of particles that are either gamma rays or electrons. We parameterise the electron flux per unit energy and solid angle as

$$\frac{\mathrm{d}^2\phi}{\mathrm{d}E\mathrm{d}\Omega} = 1.17 \times 10^{-11} \left(\frac{E}{\mathrm{TeV}}\right)^{-\Gamma} (\mathrm{GeV\,cm^2\,s\,sr})^{-1} \,, \tag{4.1}$$

with $\Gamma = 3.0$ for $E < 1\,\mathrm{TeV}$, and $\Gamma = 3.9$ for $E > 1\,\mathrm{TeV}$ [49, 50].

Interactions between CR protons and the Earth's atmosphere initiate hadronic air showers, which are generally very different from electromagnetic showers. The initial hadronic interaction produces a large number of relatively slow pions. About 1/3 are neutral pions that decay into photon pairs and initiate electromagnetic sub-showers, whereas the other 2/3 are charged pions, which either decay and dump most of their energy into neutrinos, or interact again. The resulting shower is much more widely distributed than those initiated by gamma rays, allowing the shower shape to be used as a means for discriminating between electromagnetic and hadronic showers. Hadronic CRs are however far more numerous than CR electrons and gamma rays. The corresponding proton rejection factor (*i.e.* the fraction of incoming protons that are incorrectly identified as photons/electrons) is of the order $\epsilon_p \sim 10^{-2}$ to 10^{-1} for current instruments. The electrons produced in electromagnetic cascades from neutral pion decay are the dominant contributors to the detectable Cherenkov light. This means that if a cosmic-ray proton with a given energy is mistakenly reconstructed as a gamma-ray, the gamma-ray is usually reconstructed to have roughly a third as much energy as the actual incoming proton.

Here we adopt the proton flux per unit energy and angle [51]

$$\frac{\mathrm{d}\phi}{\mathrm{d}E\mathrm{d}\Omega} = 8.73 \times 10^{-9} \left(\frac{E}{\mathrm{TeV}}\right)^{-2.71} (\mathrm{GeV\,cm^2\,s\,sr})^{-1} \,, \tag{4.2}$$

which we shift to lower energies by a factor of 3 to account for the reduced Cherenkov light emitted by hadronic showers [52]. We note that in principle heavier CR species are relevant, especially He, but these can be effectively accounted for by increasing the adopted proton rejection factor.

Throughout the present analysis, we will adopt a proton cut efficiency of $\epsilon_p = 10^{-2}$ for definiteness. We checked that with this value we can reproduce the background rates shown in Ref. [41] for Array I to within a factor of two, for energies of up to 10 TeV. We note that even for $\epsilon_p = 0$, the background rates would remain practically unchanged at energies below 2 TeV, as at these energies the background is dominated by cosmic ray electrons. We also checked that with our assumptions we can reproduce the point source sensitivity for Array I to within a factor of two below 100 GeV, and within a few tens of percent above. As formal gamma-ray and CR electron efficiencies we adopt $\epsilon_\gamma = \epsilon_e = 1$, and note that these values (along with ϵ_p) are defined with respect to the effective area of Array I from Ref. [41].

In Fig. 2, we show the contributions from CR electrons and protons assuming $\epsilon_p = 10^{-2}$, and their sum. Note that in the highest energy range that we consider in this work, 6.7 to 10 TeV, 100 hr of CTA observations lead to approximately 7.0×10^3 or 1.5×10^3 CR background events in the OFF and ON regions, respectively. For comparison we also show the gamma-ray flux from a reference DM annihilation signal, based on a thermal annihilation cross section and a DM mass of 1 TeV, within the ON and OFF regions employed in our version of the Ring method (*cf.* Section 3). The CR foreground is stronger than the DM signal by 2–3 orders of magnitude. Fig. 2 also shows a reference GDE gamma-ray background spectrum, which we discuss next.

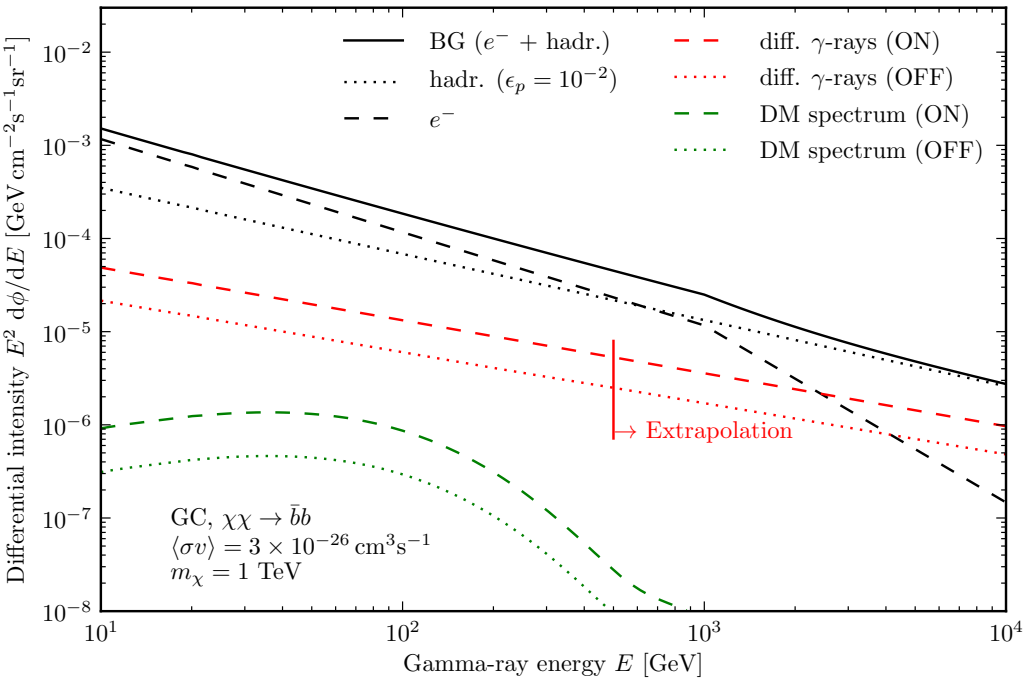

Figure 2. Background fluxes relevant for our analysis. Isotropic CR backgrounds are shown in black: protons with an assumed cut efficiency of $\epsilon_p = 10^{-2}$ (black dotted), electrons (black dashed), and total isotropic CR backgrounds (black solid). Galactic diffuse emission (GDE) is shown in red, and an example spectrum of DM annihilating to gamma-rays via $b\bar{b}$ is shown in green. We give the DM and GDE curves for the ON and OFF regions defined in the Ring Method, as described in Section 3. Beyond 500 GeV, we extrapolate the GDE spectrum using a simple power law.

4.2 Diffuse gamma-ray background

In 2006 the HESS telescope discovered diffuse gamma-ray emission from the GC at energies of 0.2–20 TeV [53]. The emission was found to be correlated with molecular clouds in the central 200 pc of the Milky Way, and is confined to Galactic latitudes $|b| < 0.3°$ and longitudes $|\ell| < 0.8°$. The spectrum suggests a hadronic origin. The absence of evidence for diffuse emission outside this window strongly influenced the choice of search regions for DM signals in previous analyses [34, 36].

Below 100 GeV, the GDE has been measured extremely well by the *Fermi*-LAT [54]. At these energies, it is expected to be dominated by π^0 decay from proton-proton interaction and bremsstrahlung. Diffuse gamma rays below 100 GeV are an important background in searches for TeV-scale DM, particularly with CTA, which will have an energy threshold of tens of GeV.

To estimate the amount of GDE in different sky regions, and to study its impact on DM searches at the GC, we adopt the P7V6 GDE model by the LAT team. This model extends up to 500 GeV, above which we use a simple power-law extrapolation.[5] We leave a more detailed study of prospects for a combined CTA + *Fermi*-LAT diffuse analysis for

[5]This is not relevant to our discussion except at very high DM masses, close to 10 TeV. See http://fermi.gsfc.nasa.gov/ssc/data/access/lat/BackgroundModels.html for details on the BG model.

future work.

In Fig. 2, we show the contribution that we inferred from this particular GDE model in the ON and OFF regions. For 100 hr of CTA observations, at energies of 6.7–10 TeV this corresponds to about 1.2×10^3 and 4.9×10^2 events respectively in the OFF and ON regions. This is a factor of ten higher than the reference DM signal at its peak value, and larger in the ON than in the OFF region. For these reasons, the GDE is a very important background that should not be neglected in DM searches at the GC.

5 Analysis

5.1 Analysis regions and J factors

For our version of the Ring method, we begin with the standard annulus of Ref. [36], with an inner radius r_1 and outer radius r_2. The centre of this annulus is offset from the GC ($b_0 = \ell_0 = 0°$) by some Galactic latitude b. We then consider a circular region centred on the GC, with some radius $\Delta_{\rm cut}$. The area in which the annulus and this circular region intersect is what we refer to as the 'ON' region. The 'OFF' region consists of the remaining part of the annulus, outside the central disc. We adopt the parameters optimised for Array E in Ref. [36]: $b = 1.42°$, $r_1 = 0.55°$, $r_2 = 2.88°$ and $\Delta_{\rm cut} = 1.36°$. Further, we exclude the Galactic disc within $|b| \leq 0.3°$ from both the ON and OFF regions, as per Ref. [36]. The resulting two RoIs can be seen in the left panel of Fig. 1. The corresponding solid angles and J factors are $\Delta\Omega_{\rm ON} = 1.2 \times 10^{-3}\,{\rm sr}$, $\Delta\Omega_{\rm OFF} = 5.6 \times 10^{-3}\,{\rm sr}$, $J_{\rm ON} = 7.4 \times 10^{21}\,{\rm GeV^2\,cm^{-5}}$ and $J_{\rm OFF} = 1.2 \times 10^{22}\,{\rm GeV^2\,cm^{-5}}$.

For our morphological analysis, we take the area covered by these two RoIs, and divide it into $1° \times 1°$ squares. We horizontally merge the various leftover regions resulting from this dissection into adjacent regions, yielding a total of 28 RoIs. These spatial bins are shown in the right panel of Fig. 1.

For comparison, we also consider DM annihilation in the Draco dwarf spheroidal galaxy, which, to a good approximation, is a point source to both CTA and *Fermi* at low energies (in the upper parts of their respective energy ranges, both would observe Draco as a somewhat extended source). For this analysis, we use the J-factor and solid angle from Table 1 of Ref. [29]: $\Delta\Omega_{\rm Draco} = 2.4 \times 10^{-4}\,{\rm sr}$, $J_{\rm Draco} = 6.31 \times 10^{18}\,{\rm GeV^2\,cm^{-5}}$.

5.2 Statistical framework

We use a binned Poisson likelihood function for comparing a DM model $\boldsymbol{\mu}$ to (mock) data $\boldsymbol{n}$

$$\mathcal{L}\left(\boldsymbol{\mu}|\boldsymbol{n}\right) = \prod_{i,j} \frac{{\mu_{ij}}^{n_{ij}}}{n_{ij}!} \exp(-\mu_{ij}). \tag{5.1}$$

Here the predictions of model $\boldsymbol{\mu}$ are the number of events μ_{ij} in the ith energy bin and the jth RoI, which are compared to the corresponding observed counts n_{ij}. We use 15 logarithmically-spaced energy bins, extending from 25 GeV to 10 TeV. Depending on the analysis (Ring or morphological), we use either two (Ring) or 28 (morphological) spatial bins (*i.e.* RoIs).

Each model prediction is composed of 3 parts: a gamma-ray signal resulting from DM annihilation (Eq. 3.5), an isotropic cosmic-ray background, and the GDE. In our statistical analysis each of these components can be rescaled via a parameter: $\langle\sigma v\rangle$ for the DM gamma-ray signal, and linear rescaling factors $R_{\rm CR}$ and $R_{\rm GDE}$ for the isotropic cosmic-ray background

and the GDE respectively,

$$\mu_{ij} = {\mu_{ij}}^{\rm DM} + {\mu_{ij}}^{\rm CR} R_{{\rm CR},i} + {\mu_{ij}}^{\rm GDE} R_{{\rm GDE},i}. \tag{5.2}$$

Because the CR flux is isotropic to a good approximation, the $\mu_{ij}^{\rm CR}$s are trivially related by $\mu_{ij}^{\rm CR}/\mu_{ik}^{\rm CR} = \Omega_j/\Omega_k$, where Ω_j denotes the angular size of the jth RoI. Note that we do not vary the relative normalisations of the CR electron and proton spectra, only their sum. We also do not allow the GDE to be rescaled independently in each RoI, as this would simply allow the GDE to adjust to the data in its entirety in every bin, effectively non-parametrically.

Systematic uncertainties in the signal rates can be accounted for by multiplying the predicted signals μ_{ij} by scaling parameters α_{ij} and β_i, then profiling the likelihood over their values. We assume Gaussian nuisance likelihoods for all α and β, with respective variances σ_α^2 and σ_β^2 independent of i and j. Strictly, the distributions should be log-normal so that they go smoothly to zero as α and β go to zero, but for small σ this makes practically no difference; typical values of σ that we will consider in the following section are ≤ 0.03, well within the range where this is a good approximation. With these scaling parameters, the likelihood function becomes

$$\mathcal{L}\left(\boldsymbol{\mu}, \boldsymbol{\alpha}, \boldsymbol{\beta} | \boldsymbol{n}\right) = \prod_i \frac{1}{\sqrt{2\pi}\sigma_\beta} e^{-\frac{(1-\beta_i)^2}{2\sigma_\beta^2}} \prod_j \frac{(\mu_{ij}\alpha_{ij}\beta_i)^{n_{ij}}}{\sqrt{2\pi}\sigma_\alpha \cdot n_{ij}!} e^{-\mu_{ij}\alpha_{ij}\beta_i} e^{-\frac{(1-\alpha_{ij})^2}{2\sigma_\alpha^2}}. \tag{5.3}$$

This formulation accounts for systematic uncertainty on any factor that enters linearly in the calculation of the total signal, such as effective area. The parameters α_{ij}, which vary across both energy bins and RoIs, account for *e.g.* uncertainties related to non-uniformities in the acceptance of CTA within a FoV. We will refer to all uncertainties described by α_{ij} as *differential acceptance uncertainties*. Reasonable values for σ_α are of the order of a few percent [55, 56]. The parameters β_i, on the other hand, describes systematic uncertainties for a given energy that apply equally over the whole FoV.

Here we are most interested in the cross-RoI systematics, as systematics that apply equally across the whole FoV will essentially just degrade an entire $n\sigma$ confidence-level sensitivity curve by an offset of less than $n\sigma_\beta$ (although the rescaling could differ with energy, if σ_β were permitted to vary with energy). We therefore investigate the impacts of allowing each α_{ij} to vary independently, and simply set $\beta_i = 1$ for all i. The impacts of *e.g.* an energy-dependent systematic uncertainty on the *Fermi* or CTA effective areas could be easily accounted for by also profiling over each β_i.

Taking the likelihood function Eq. (5.3), we perform a maximum likelihood analysis across α_{ij}, $\langle\sigma v\rangle$, $R_{\rm CR}$, and in certain cases, $R_{\rm GDE}$. We can determine the maximum likelihood value of α_{ij} simply by solving

$$\frac{{\rm d}\mathcal{L}\left(\mu_{ij}, \alpha_{ij}, \beta_i | n_{ij}\right)}{{\rm d}\alpha_{ij}} = 0, \tag{5.4}$$

and demanding that α_{ij} be positive. This gives

$$\alpha_{ij} = \frac{1}{2}\left(1 - \sigma_\alpha^2\mu_{ij}\beta_i + \sqrt{1 + 4\sigma_\alpha^2 n_{ij} - 2\sigma_\alpha^2\mu_{ij}\beta_i + \sigma_\alpha^4 {\mu_{ij}}^2 {\beta_i}^2}\right). \tag{5.5}$$

The mock data $\boldsymbol{n}$ that we use for deriving sensitivities in the following section assume a fixed isotropic cosmic-ray background component with $R_{{\rm CR},i} = 1$ in all bins, and no

contribution from DM annihilation. Depending on the analysis, we either include no GDE ($R_{\mathrm{GDE},i} = 0$ for all i) in the mock data, or a fixed GDE with $R_{\mathrm{GDE},i} = 1$. The mock data sets that we employ are not Poisson realisations of a model with these assumptions, but rather simply the expectation number of events given these assumptions; this has been referred to as the "Asimov data set" [57].

We calculate 95% confidence level (CL) upper limits by increasing the signal flux (or annihilation cross-section) from its best-fit value, whilst profiling over the remaining parameters, until $-2\ln\mathcal{L}$ changes by 2.71. In the case of the differential point-source sensitivity that we discuss in the next section, for a 95% CL upper limit we also require at least one energy bin to contain at least 3.09 events [58]. In this calculation, we determine background rates over the 80% containment region of the PSF, following *e.g.* Ref. [41]. Note that we neglect instrumental systematics when evalulating *Fermi*-LAT sensitivities (setting $\alpha_{ij} = \beta_i = 1$).

5.3 Background treatment

In both our Ring and morphological analyses, we allow the isotropic cosmic-ray background rescaling factor $R_{\mathrm{CR},i}$ to vary between 0.5 and 1.5 in our fits. We then profile the likelihood over this parameter in each energy bin.

Including the GDE in our analysis is more complicated, as in principle, the data-driven GDE model derived by *Fermi* could already contain some contribution from DM annihilation. Therefore, to gauge the impact of the diffuse emission upon current analysis methods, for our analysis with the Ring method we inject the GDE into our mock dataset $\boldsymbol{n}$, with $R_{\mathrm{GDE},i} = 1$ in all bins. We then carry out a full analysis with a model $\boldsymbol{\mu}$ where the GDE normalisation is left free to vary, *i.e.* $R_{\mathrm{GDE},i}$ is left free in the fits, but we require it to be non-negative. The idea in this exercise is to leave the analysis method as much as possible unaltered relative to previous analyses, but to make the mock data fed into the method more realistic. Leaving the GDE free to vary in each energy bin produces the most conservative constraints and avoids assumptions on the GDE energy spectrum. The results of this analysis are given in Sec. 6.2.

Our morphological analysis allows a more refined inclusion of GDE. Using more than two RoIs allows us to better exploit the shape differences between the GDE, which is concentrated along the Galactic plane, and the DM annihilation signal, which is spherically distributed around the GC. For this analysis we again include the GDE in the mock data with $R_{\mathrm{GDE}} = 1$ in all bins, and allow the individual $R_{\mathrm{GDE},i}$ values to vary in each energy bin. To implement this analysis we use lookup tables: for each DM mass, and each energy bin and RoI, we consider a range of DM cross-sections. For each cross-section value, we calculate the maximum likelihood point when profiling numerically over R_{BG} and R_{GDE}, and analytically over all α_{ij} using Eq. (5.5). Storing these values then gives us a partial likelihood as a function of cross-section in that bin, for each DM mass. For a given DM mass, we can then combine the partial likelihoods in different bins to determine cross-section limits at arbitrary confidence levels. The results of this analysis are given in Sec. 6.3 and 6.4.

6 Results

To keep the discussion as independent from specific DM scenarios as possible, in this section we will often quote the *differential sensitivity*, which is the sensitivity to a signal in an isolated energy bin. This measure is commonly used in the gamma-ray community (see *e.g.* Ref. [55]).

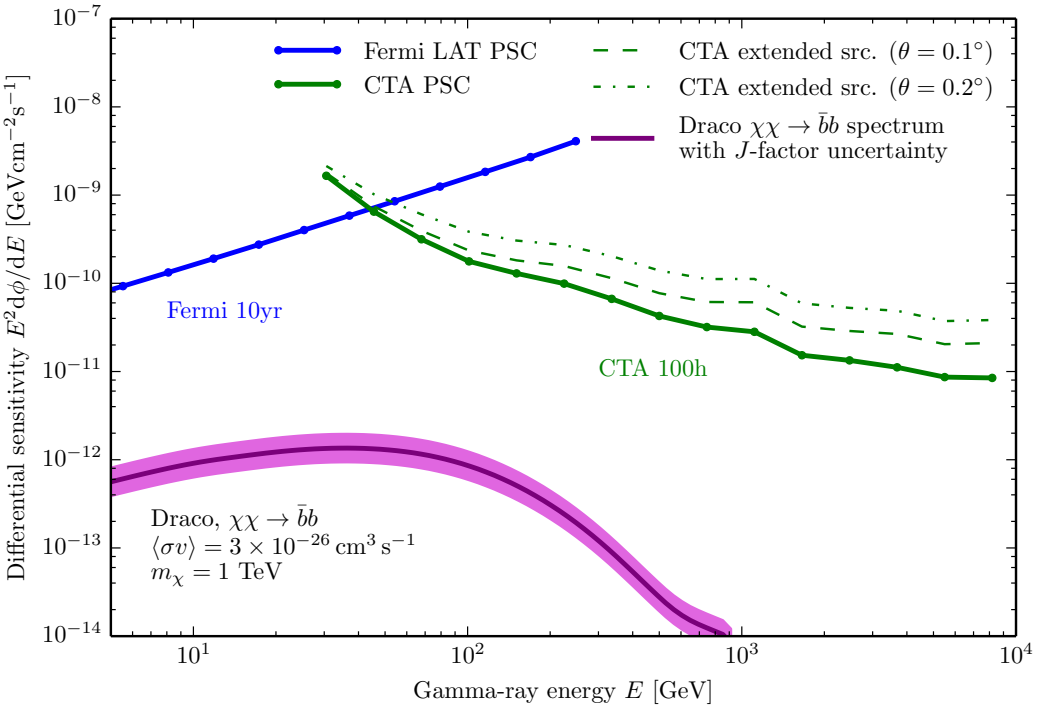
Fermi LAT PSC
CTA PSC
CTA extended src. ($\theta = 0.1°$)
CTA extended src. ($\theta = 0.2°$)
Draco $\chi\chi \to \bar{b}b$ spectrum with J-factor uncertainty
Fermi 10yr
CTA 100h
Draco, $\chi\chi \to \bar{b}b$
$\langle\sigma v\rangle = 3 \times 10^{-26}\,\mathrm{cm}^3\,\mathrm{s}^{-1}$
$m_\chi = 1$ TeV
Differential sensitivity $E^2\mathrm{d}\phi/\mathrm{d}E$ [GeVcm^{-2}s^{-1}]
Gamma-ray energy E [GeV]

Figure 3. Differential sensitivity of *Fermi*-LAT (blue) and CTA (green) point source observations, in terms of 95% CL upper limits. The *Fermi*-LAT differential sensitivity assumes an observation time of 10 years, with energy bins of $\Delta \log_{10} E = 0.165$ size between $E = 5.0\,\mathrm{GeV}$ and 300 GeV, and includes only statistical errors. The CTA sensitivities assume an observation time of 100 hours, include 1% differential acceptance uncertainty, with bins of $\Delta \log_{10} E = 0.173$ size between $E = 25\,\mathrm{GeV}$ and 10 TeV. Sensitivities for extended sources of different sizes are also shown for CTA (green dashed and dot-dashed). The DM annihilation spectrum from the Draco dwarf galaxy uses a J-factor of $6.31^{+3.24}_{-1.94} \times 10^{18}\,\mathrm{GeV}^2\mathrm{cm}^{-5}$ from Table 1 of [29], with the band covering the uncertainty range.

Here we consider energy bins with a width of $\simeq 0.17$ dex (approximately six bins per decade), and quote sensitivities in terms of projected one-sided 95% CL upper limits.

We will start with a discussion of the point source sensitivity, which is relevant for DM searches in dwarf spheroidal galaxies. The remaining part of this section will then discuss DM searches at the GC. Finally, we will present projected upper limits on the DM annihilation cross-section for various annihilation channels and DM profiles.

6.1 Point source sensitivity

Some of the most powerful targets for indirect DM searches with gamma rays are dwarf spheroidal galaxies. In order to compare the potential of CTA with the abilities of current instruments like *Fermi*-LAT, it is instructive to consider their differential point source sensitivity. In Fig. 3, we show the differential sensitivity of CTA, assuming an observation time of 100 hours, compared to the one of *Fermi*-LAT after ten years of observation (assuming 20% of the time is spend on the source). Due to its much larger effective area, CTA will outperform *Fermi*-LAT at energies above about 100 GeV, where *Fermi* becomes limited by photon statistics.

For comparison, we show the signal flux expected from the dwarf spheroidal galaxy Draco, in the case of a DM particle with $m_\chi = 1\,\mathrm{TeV}$ mass, annihilating into $b\bar{b}$ final states with an annihilation cross section of $\langle\sigma v\rangle = 3 \times 10^{-26}\,\mathrm{cm}^3\,\mathrm{s}^{-1}$. Draco is one of the most promising targets, and the envelope shows the uncertainty in the projected signal flux, which is primarily related to its overall mass (taken from Ref. [29]).

Dwarf spheroidal galaxies have half-light radii of a few times 0.1° (see *e.g.* Ref. [59]), and at high energies will appear as extended sources for CTA. For comparison, we show the impact on the expected sensitivity in Fig. 3. We derive these sensitivity curves by assuming that a dwarf is observed by CTA to have an angular extent given by the sum in quadrature of the 68% PSF containment radius and the intrinsic angular extent indicated in the figures. This effect will degrade the sensitivity by a factor of a few at TeV energies. As can be seen in Fig. 3, for a gamma-ray spectrum from hadronic processes like annihilation into $b\bar{b}$, CTA will outperform *Fermi* for DM masses above about 1 TeV. However, the sensitivity of CTA will still fall about two orders of magnitude short of testing the canonical thermal cross-section.

In order to understand how the limits scale with observing time, it is helpful to realise that in this transition regime the limiting factor for CTA is the enormous background of CR electrons (and to a lesser degree unrejected protons and light nuclei; see Fig. 2). These CR electrons can easily swamp weak sources even if the number of events that are detected from the source is much larger than in case of *Fermi*-LAT. Indeed, apart from the difference in the effective area, the main difference between space-based and ground-based gamma-ray telescopes is their respective abilities to reject backgrounds. This is relatively simply realised by an anti-coincidence detector in the case of *Fermi*, but extremely challenging in the case of Cherenkov Telescopes like CTA. This means that even a larger observing time with CTA would not significantly affect the point-source sensitivity at the low energies relevant for TeV DM searches. In contrast, much longer observation times with space-based and practically background-free instruments like *Fermi* could (at least in principle) improve on existing limits by orders of magnitude.

6.2 Galactic centre sensitivity with Ring method

The most intense signal from DM annihilation is expected to come from the GC. The large CR background will in that case be of lesser relevance than for observations of dwarf spheroidal galaxies, making the GC a particularly promising target for CTA. Previous analyses found that CTA will improve existing limits (with the strongest ones coming currently from HESS) by an order of magnitude or so [36–38]. However, all existing analyses have neglected the impact of the GDE, which is strongest in the direction of the Galactic center. We will demonstrate here that this in fact has a significant impact on DM searches with CTA.

In Fig. 4, we show the differential sensitivity for a DM signal in the GC that we obtain when using our version of the Ring method ([36], *cf.* Fig. 1), under various assumptions about the GDE and instrumental systematics. When creating mock data for our baseline analysis, we include individual estimates for the GDE in the different RoIs. The Ring method is only sensitive to integrated fluxes measured in the ON and OFF regions. In our likelihood fit to the mock data the normalisations of the DM and the GDE components are therefore degenerate, as these two components in general contribute a larger flux to the ON than the OFF region – whereas variations in the average intensity in both regions can be absorbed by slight changes in the CR background normalisation. An increased DM contribution can be compensated for by a smaller GDE contribution, and vice versa. This degeneracy breaks

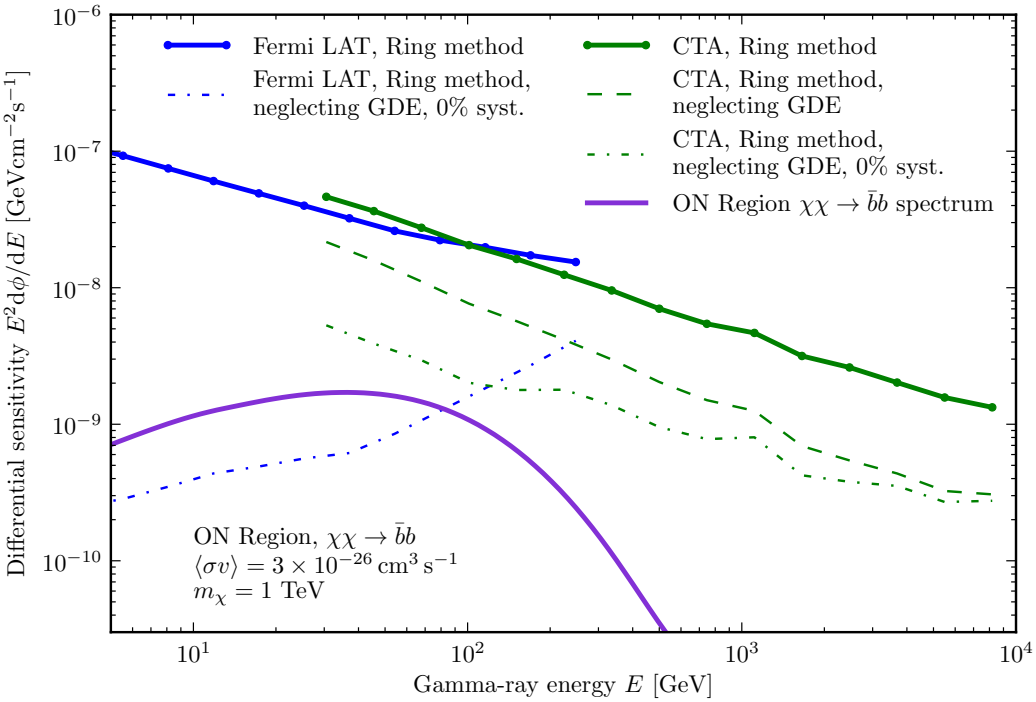
Fermi LAT, Ring method
Fermi LAT, Ring method, neglecting GDE, 0% syst.
CTA, Ring method
CTA, Ring method, neglecting GDE
CTA, Ring method, neglecting GDE, 0% syst.
ON Region $\chi\chi \to \bar{b}b$ spectrum
ON Region, $\chi\chi \to \bar{b}b$
$\langle\sigma v\rangle = 3 \times 10^{-26}\,\mathrm{cm}^3\,\mathrm{s}^{-1}$
$m_\chi = 1$ TeV
Differential sensitivity $E^2\mathrm{d}\phi/\mathrm{d}E$ [GeVcm^{-2}s^{-1}]
Gamma-ray energy E [GeV]

Figure 4. Differential sensitivity of *Fermi*-LAT (blue) and CTA (green) for GC observations, using the Ring method as defined in Section 3. The two upper solid lines show our baseline estimate for the sensitivity, with galactic diffuse emission and a differential acceptance uncertainties of 1% included. For comparison, the dashed green line shows the differential sensitivity for CTA neglecting the GDE, but still including systematics of 1%; the dash-dotted lines in blue and green show the differential sensitivity for *Fermi*-LAT and CTA respectively, neglecting GDE and instrumental systematics. Observation times and energy binning are the same as in Fig. 3. The purple line shows the gamma-ray spectrum from the ON region assuming a DM mass of 1 TeV and an annihilation cross section of $\langle\sigma v\rangle = 3 \times 10^{-26}\mathrm{cm}^3\mathrm{s}^{-1}$ to $b\bar{b}$, using the Einasto profile from Eq. (3.2).

when the GDE contribution drops to zero, at which point the $-2\ln\mathcal{L}$ increases with increasing DM annihilation cross-section, which then leads to a conservative upper limit on the DM flux.

The curves that we show in Fig. 4 where the GDE has not been included are based on neglecting GDE in the the mock data and the subsequent analysis (setting $R_{\mathrm{GDE}} = 0$ everywhere). We see here that in the case of the Ring method, neglecting the GDE artificially improves the projected sensitivity by a factor of up to 5. Furthermore, neglecting instrumental systematics (as in Ref. [37]) increases the sensitivity again by another factor of a few. For comparison, we again show the flux expected from a DM particle with 1 TeV mass, annihilating into $b\bar{b}$ at the canonical thermal rate.

6.3 Galactic centre sensitivity with multi-bin morphological method

It is instructive to see the results that one would obtain by applying the Ring method to *Fermi*-LAT instead of CTA data. As shown in Fig. 4, the resulting sensitivity curve simply continues the curve from CTA to lower energies. This can be readily understood, as in both cases the actual limits are driven by the same GDE. We can see that the GDE is the factor holding back the Ring analysis. This motivates us to consider a procedure capable of taking

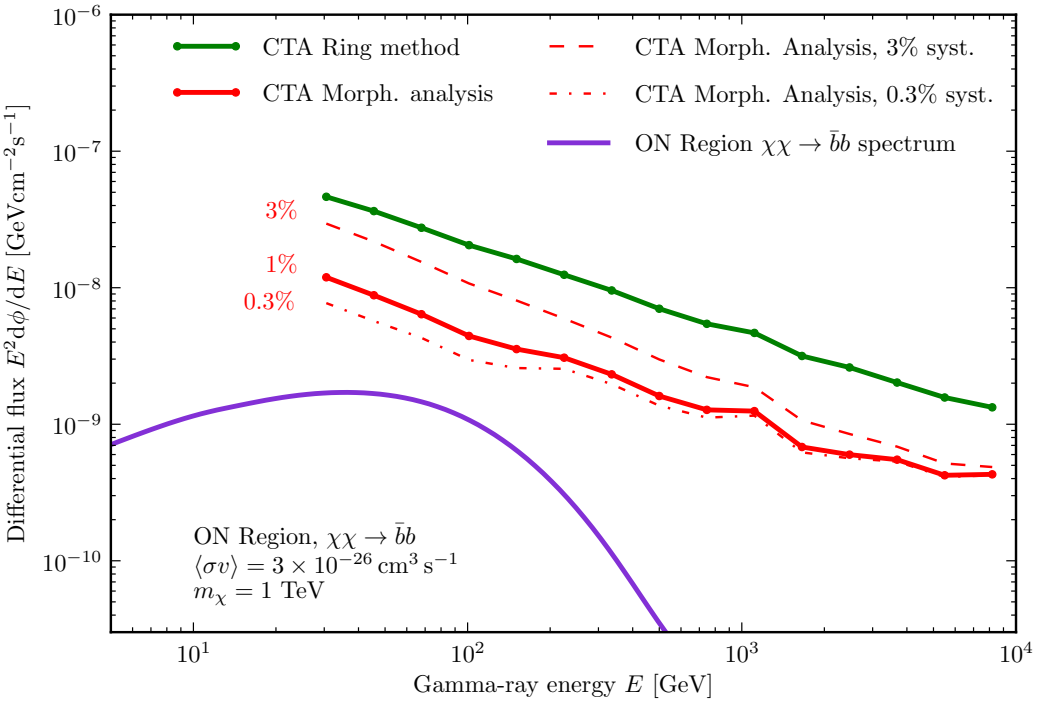

Figure 5. Same as Fig. 4, but comparing our previous Ring analysis (green) with our morphological analysis (red), again assuming 100 hr of observation. The solid lines show our baseline estimate for the sensitivity of the two analysis methods, with galactic diffuse emission included and differential acceptance uncertainties of 1%. Also shown are sensitivities produced using the morphological analysis including GDE but using systematics of 3% (dashed) and 0.3% (dash-dotted).

into account morphological differences between the GDE and DM signal, which is what we discuss next.[6]

Here we take an important first step towards an improved DM search strategy for CTA by proposing a morphological analysis of the gamma rays from the GC. We will estimate the *most optimistic* limits that one can obtain on DM annihilation in the presence of the known GDE, assuming that the morphology of the GDE is perfectly understood. To this end, we define the 28 subregions distributed as shown in the right panel of Fig. 1. They are all part of the original RoI from the Ring method. This has the advantage that the required observation strategy and results are directly comparable.

Fig. 5 shows that with our morphological analysis, the projected differential sensitivity is better by a factor of four than what can be obtained with the Ring method. Note that the limiting factor in our results, at least for sub-TeV energies, is now not the GDE but differential acceptance uncertainties, namely relative systematic uncertainties in the photon acceptance in different regions of the *same* FoV. For this uncertainty, we assume 1% throughout, which is a rather realistic value. This might however vary by a factor of a few up or down, depending on the experimental details (*cf.* Sec. 5.2). Indeed, varying the systematic uncertainty in a

[6]Considering the energy spectrum of the signal as we do here of course also improves CTA limits [38]; all our analyses are carried out including this information. Once a signal is detected however, if gamma-ray lines or virtual internal Bremsstrahlung seem relevant, a primarily spectral analysis would be preferable [60, 61].

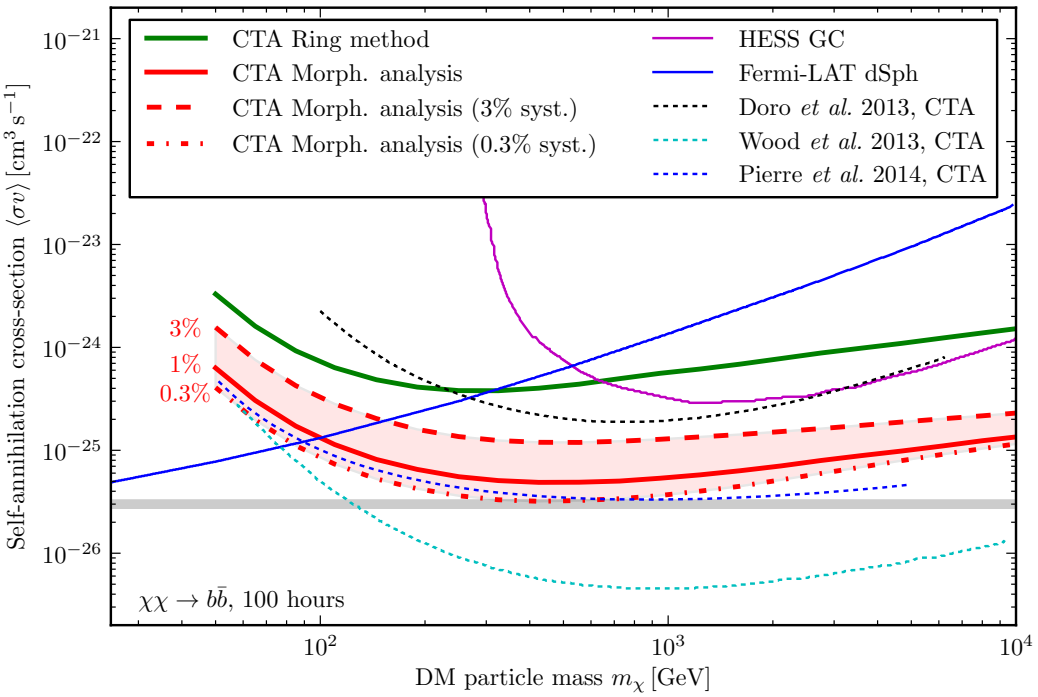

Figure 6. Upper limits on the DM annihilation cross section using the previous Ring method (green) and our morphological analysis (red), assuming 100 hr of observation of the GC. The thick solid green and red lines are our baseline estimates of the limits attainable using the two analysis methods, assuming differential acceptance uncertainties of 1% and including GDE. The red dashed and dot-dashed lines show the limits produced in the morphological analysis assuming 3% and 0.3% systematics, respectively. Also shown are current limits on the DM annihilation cross section (thin solid lines; *Fermi*-LAT dwarf analysis in blue [29], HESS GC observations in pink [34]), as well as various projected CTA limits (thin dotted lines; Doro *et al.* 2013 in black [36], Wood *et al.* 2013 in cyan [37], and Pierre *et al.* 2014 in dark blue [38]). For the sake of comparison, the CTA projections are rescaled to 100 hr observation time and our adopted Einasto profile.

reasonable range has a significant impact on the actual projected constraints.[7]

6.4 Projected cross-section limits

We now present our results in terms of limits on DM annihilation, in the common $\langle\sigma v\rangle$-vs-mass plane, assuming DM annihilation into different final states with a branching ratio of 100%. First we provide some context by summarising the most relevant previous work.

In Fig. 6, we show existing experimental limits from the *Fermi*-LAT satellite [29] and the HESS telescope [34], on DM annihilation into $b\bar{b}$. In this figure, all limits from the GC are rescaled to our baseline Einasto DM profile. Projected limits correspond to 100 hr observation time for CTA. The *Fermi*-LAT limits reach the thermal cross section for DM

[7] Although we introduced the morphological analysis method primarily to improve limits in the presence of the GDE, we also compared its performance to that of the Ring method in the case of no GDE and 0% systematics. In this case the morphological analysis produces limits that are marginally better than those of the Ring method. This is expected, as the smaller RoIs still provide an additional constraint on the spatial distribution of the signal.

masses below about 10 GeV. The HESS limits are strongest close to 1 TeV, where they reach $3 \times 10^{25}\,\mathrm{cm}^3\,\mathrm{s}^{-1}$.

Also shown are the projected limits for CTA from Refs. [36–38]. The analysis given in Ref. [37] assumes an observation time of 500 hr, and we have rescaled their limits to account for our baseline DM profile and observation time of 100 hr. In fact, even after this rescaling, the projected limits from Ref. [37] remain the most optimistic; they apparently do not account for systematic uncertainties or the effects of the GDE, and make use of an extended array with 61 mid-sized telescopes. This extended array is assumed to contain 36 extra mid-sized telescopes, as an additional, rather speculative, US contribution on top of the baseline array.

The limits presented in Ref. [36] include no GDE and no spectral analysis. They were built upon a profile derived from the Aquarius simulation, and therefore include an effective substructure boost compared to a regular NFW profile. We have removed this boost in order to allow direct comparison with our results, and those of others. The inclusion of substructure increases the J-factor and thus also the signal, which results in a stronger limit. As we use identical regions of interest to those of [36], we can estimate the substructure boost factor by comparing ON region J-factors: [36] give their result as $J_{\mathrm{ON,Aq.}} = 4.68 \times 10^{22}\mathrm{GeV}^2\mathrm{cm}^{-5}$, while our smooth Einasto profile (Sec. 3) gives $J_{\mathrm{ON,\ Ein.}} = 7.41 \times 10^{21}\mathrm{GeV}^2\,\mathrm{cm}^{-5}$. This yields a boost factor of 6.31; we hence multiply the limits of Ref. [36] by this factor for presentation in Fig. 6.

The limits presented in Ref. [38] are derived in a similar fashion to the Ring method ones in the present analysis, including spectral analysis, but neglect contributions from the GDE, systematics and proton CRs.

Our projected CTA upper limits on the annihilation cross-section using our version of the Ring method are shown in Fig. 6 by the thick green line. In contrast to Ref. [36], we *include* the expected GDE as discussed above (*cf.* Fig. 5). As a consequence, we find somewhat weaker limits at intermediate masses than in this previous work. The different shape of the limits as function of mass is due to our lower energy threshold, and the fact that we carry out a spectral analysis, whereas Ref. [36] used only one large energy bin. This consequence of including spectral information was noted previously in Ref. [38], whose limits have a very similar shape to our own. The normalisation difference between our results and those of Ref. [38] can be explained primarily by our inclusion of GDE and differential acceptance uncertainties, and to a lesser extent by the different array configurations assumed in the two papers. The fact that our limits are almost two orders of magnitude weaker than those of Ref. [37] is primarily due to the unrealistic array considered in that paper, and our inclusion of GDE and systematics.

Interestingly, our projected constraints are actually also weaker than the existing limits from HESS, which are based on 112 hours of GC observations. This difference is likely due to two things. The first is simply that the RoIs adopted in the Ring method and in the HESS analysis are rather different. The second is that the HESS analysis is a true ON-OFF analysis, which neglects the GDE by definition; this was only possible to do in a valid way in the HESS analysis due to the instrument's high energy threshold and the fact that at such energies, the GDE intensity observed by *Fermi*-LAT happens (by chance?) to be very similar in the rather complicated ON and OFF regions chosen by HESS.

Most importantly, moving from the Ring method to our morphological analysis yields *a sensitivity improvement by up to an order of magnitude*. We show in Fig. 6 that morphological analysis improves the projected limits by up to a factor of ten for high DM masses compared

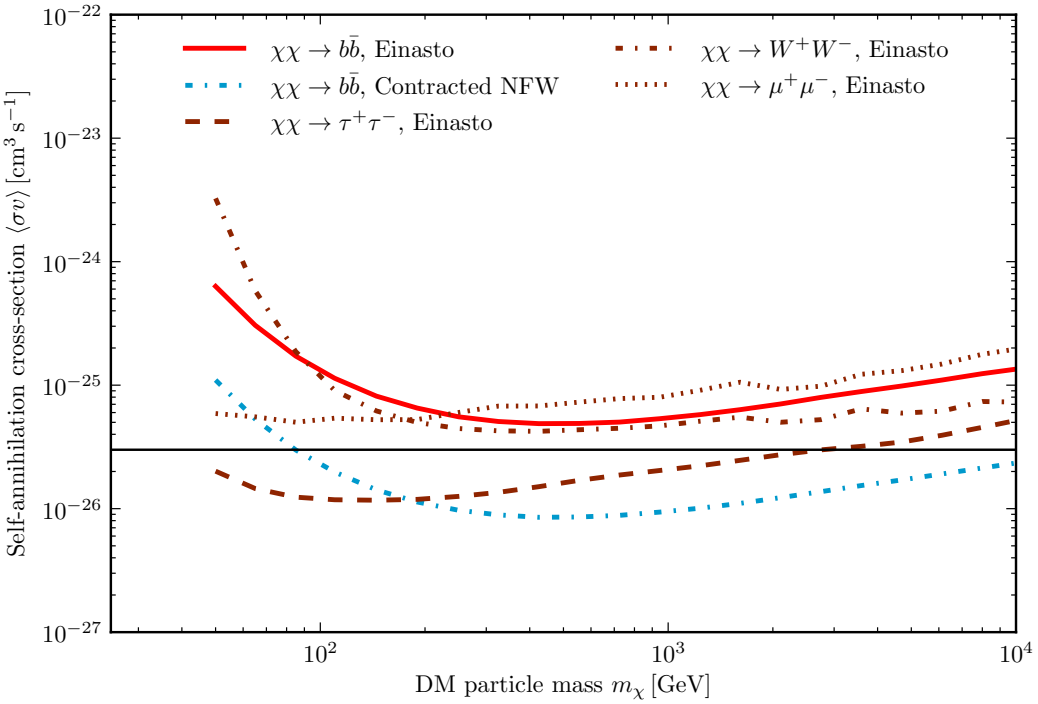

Figure 7. Comparison of $\langle\sigma v\rangle$ limits from CTA observations of the GC, assuming different annihilation channels and DM halo profiles. Einasto lines assume the main halo profile described in Sec. 3. The contracted NFW profile with an inner slope of $\gamma = 1.3$ can also be found in that section. All lines assume 1% systematics, 100 hr of observations and include GDE.

to the Ring method.[8] This is mostly due to the fact that the large number of subregions allows an efficient discrimination between the morphology of the GDE and a putative DM signal. Note that the projected limits again depend critically on instrumental systematics, and as indicated by the band in Fig. 6. This is due to the large number of measured events in the RoIs. For our baseline DM profile, we find that the thermal annihilation cross section can be only reached if instrumental systematics (namely differential acceptance uncertainties as discussed above) are under control at the sub-percent level. At the same time, increasing the time over which the GC is observed by CTA will have a negligible effect on the projected limits.

Finally, we discuss how the projected limits depend on the adopted annihilation channel or DM halo profile. These results are shown in Fig. 7. Besides our baseline scenario, where we assumed an Einasto profile and annihilation into $b\bar{b}$ final states, we show limits for annihilation to $\tau^+\tau^-$, W^+W^- and $\mu^+\mu^-$ with an Einasto profile, and to $b\bar{b}$ with an alternative density profile.[9] We find that in the case of annihilation via the $\tau^+\tau^-$ channel, CTA would be able to probe annihilation cross-sections well beyond the thermal value even for a standard Einasto profile. In the case of a contracted NFW profile with a inner slope of $\gamma = 1.3$, as described

[8] This is not directly apparent from Fig. 5, where the difference is merely a factor of four. The reason is that a DM signal would appear in several energy bins simultaneously, which strengthens the limits in the case where the GDE is correctly modelled.

[9] Note that fluctuations of the limits, which are most visible in the cases of $\mu^+\mu^-$ and W^+W^- final states with strong final state radiation, come from variations in the adopted effective area.

in Sec. 3, the J-factor increases by a factor of 2.9 (summed over all RoIs). If this profile is indeed realised in nature, it would bode well for future observations with CTA, as CTA could probe well beyond the canonical thermal cross section for a large range of DM particle masses between 100 GeV and 10 TeV.

7 Conclusion

In this paper we have performed a new estimate of the CTA sensitivity to DM annihilation. Here we summarise our main conclusions:

- *Including the Galactic diffuse emission substantially degrades the sensitivity of CTA.* We have assessed the impacts of all backgrounds, including protons and electrons in cosmic-rays hitting the atmosphere and, for the first time in this type of analysis, diffuse astrophysical emission. The impact of including the galactic diffuse emission can be observed in particular in Fig. 4, where the CTA differential sensitivity is found to be substantially degraded (solid line) with respect to the case where the GDE is not included in the analysis (dashed green line).

- *Including systematic errors substantially degrades the CTA sensitivity.* In this paper we introduced a statistical framework that allowed us to account for the impact of differential acceptance uncertainties within a FoV on DM limits from CTA. This impact can be seen in Fig. 5, where the sensitivity of CTA to DM annihilation is shown for three different values of the magnitude of these systematics: 3% (dashed), 1% (solid) and 0.3% (dash-dotted).

- *A morphological analysis substantially improves the sensitivity of CTA.* Our morphological analysis allows a proper exploitation of the shape differences between the GDE, which is concentrated along the Galactic plane, and the DM annihilation signal, which is spherically distributed around the GC. The constraints derived under this approach are more stringent by a factor of a few compared to those obtained with the Ring analysis. This is best seen by comparing the red (morphological) and green (non-morphological) curves in Figs. 5 and 6.

- *Prospects for detecting WIMPs with CTA.* Our most realistic estimate of the upper limits on the DM annihilation cross section possible with 100 hr of GC observation by CTA are shown as a red solid line in Fig. 6. These correspond to a morphological analysis assuming annihilation to $b\bar{b}$, systematics of 1%, and include diffuse emission. In order to reach canonical thermal cross section, shown as a horizontal line, systematic errors should be reduced to 0.3%. If the DM profile is steeper than NFW or Einasto, the sensitivity curve drops below the thermal cross-section for a broad range of masses, as we show in Fig. 7. Here, for the same annihilation channel and a contracted profile rising as $r^{-1.3}$, CTA is found to be able to probe WIMPs with a thermal cross-section between 100 GeV and 10 TeV.

Acknowledgements. We thank Arnim Balzer, David Berge, Jan Conrad, Christian Farnier, Mathias Pierre and Jenny Siegal-Gaskins for useful discussions. PS acknowledges support from the UK Science & Technology Facilities Council, and GB from European Research Council through the ERC Starting Grant *WIMPs Kairos*.

References

[1] G. Jungman, M. Kamionkowski, and K. Griest, *Supersymmetric dark matter*, *Phys. Rep.* **267** (1996) 195–373, [hep-ph/9506380].

[2] L. Bergström, *Non-baryonic dark matter: observational evidence and detection methods*, *Rep. Prog. Phys.* **63** (2000) 793–841, [hep-ph/0002126].

[3] G. Bertone, D. Hooper, and J. Silk, *Particle dark matter: evidence, candidates and constraints*, *Phys. Rep.* **405** (2005) 279–390, [hep-ph/0404175].

[4] T. Bringmann and C. Weniger, *Gamma ray signals from dark matter: Concepts, status and prospects*, *Physics of the Dark Universe* **1** (2012) 194–217, [arXiv:1208.5481].

[5] G. Bertone, ed., *Particle Dark Matter: Observations, Models and Searches*. Cambridge University Press, 2010.

[6] Super-Kamiokande Collaboration: T. Tanaka, K. Abe, *et. al.*, *An Indirect Search for Weakly Interacting Massive Particles in the Sun Using 3109.6 Days of Upward-going Muons in Super-Kamiokande*, *ApJ* **742** (2011) 78, [arXiv:1108.3384].

[7] IceCube Collaboration: R. Abbasi, Y. Abdou, *et. al.*, *Multiyear search for dark matter annihilations in the Sun with the AMANDA-II and IceCube detectors*, *Phys. Rev. D* **85** (2012) 042002, [arXiv:1112.1840].

[8] IceCube Collaboration: M. G. Aartsen, R. Abbasi, *et. al.*, *Search for Dark Matter Annihilations in the Sun with the 79-String IceCube Detector*, *Phys. Rev. Lett.* **110** (2013) 131302, [arXiv:1212.4097].

[9] P. Scott, C. Savage, J. Edsjö, and the IceCube Collaboration: R. Abbasi et al., *Use of event-level neutrino telescope data in global fits for theories of new physics*, *JCAP* **11** (2012) 57, [arXiv:1207.0810].

[10] H. Silverwood, P. Scott, *et. al.*, *Sensitivity of IceCube-DeepCore to neutralino dark matter in the MSSM-25*, *JCAP* **3** (2013) 27, [arXiv:1210.0844].

[11] C. Rott, J. M. Siegal-Gaskins, and J. F. Beacom, *New sensitivity to solar WIMP annihilation using low-energy neutrinos*, *Phys. Rev. D* **88** (2013) 055005, [arXiv:1208.0827].

[12] P. Salati, F. Donato, and N. Fornengo, *Indirect dark matter detection with cosmic antimatter*, in Bertone [5], ch. 26, pp. 521–546. arXiv:1003.4124.

[13] O. Adriani, G. C. Barbarino, *et. al.*, *New Measurement of the Antiproton-to-Proton Flux Ratio up to 100 GeV in the Cosmic Radiation*, *Phys. Rev. Lett.* **102** (2009) 051101, [arXiv:0810.4994].

[14] L. A. Dal and M. Kachelrieß, *Antideuterons from dark matter annihilations and hadronization model dependence*, *Phys. Rev. D* **86** (2012) 103536, [arXiv:1207.4560].

[15] L. Bergström, T. Bringmann, I. Cholis, D. Hooper, and C. Weniger, *New Limits on Dark Matter Annihilation from Alpha Magnetic Spectrometer Cosmic Ray Positron Data*, *Phys. Rev. Lett.* **111** (2013) 171101, [arXiv:1306.3983].

[16] N. Fornengo, L. Maccione, and A. Vittino, *Dark matter searches with cosmic antideuterons: status and perspectives*, *JCAP* **9** (2013) 31, [arXiv:1306.4171].

[17] E. Carlson, A. Coogan, *et. al.*, *Antihelium from dark matter*, *Phys. Rev. D* **89** (2014) 076005, [arXiv:1401.2461].

[18] M. Cirelli, N. Fornengo, M. Taoso, and A. Vittino, *Anti-helium from Dark Matter annihilations*, arXiv:1401.4017.

[19] D. G. Cerdeño and A. M. Green, *Direct detection of WIMPs*, in Bertone [5], ch. 17, pp. 347–369. arXiv:1002.1912.

[20] M. Pato, L. Baudis, *et. al.*, *Complementarity of dark matter direct detection targets*, *Phys. Rev. D* **83** (2011) 083505, [arXiv:1012.3458].

[21] C. Strege, R. Trotta, G. Bertone, A. H. G. Peter, and P. Scott, *Fundamental statistical limitations of future dark matter direct detection experiments*, *Phys. Rev. D* **86** (2012) 023507, [arXiv:1201.3631].

[22] K. Freese, M. Lisanti, and C. Savage, *Annual Modulation of Dark Matter: A Review*, *Rev. Mod. Phys.* **85** (2013) 1561–1581, [arXiv:1209.3339].

[23] XENON100 Collaboration: E. Aprile, M. Alfonsi, *et. al.*, *Dark Matter Results from 225 Live Days of XENON100 Data*, *Phys. Rev. Lett.* **109** (2012) 181301, [arXiv:1207.5988].

[24] LUX Collaboration: D. Akerib *et. al.*, *First results from the LUX dark matter experiment at the Sanford Underground Research Facility*, *Phys. Rev. Lett.* **112** (2014) 091303, [arXiv:1310.8214].

[25] J. Goodman, M. Ibe, *et. al.*, *Constraints on dark matter from colliders*, *Phys. Rev. D* **82** (2010) 116010, [arXiv:1008.1783].

[26] P. J. Fox, R. Harnik, J. Kopp, and Y. Tsai, *Missing energy signatures of dark matter at the LHC*, *Phys. Rev. D* **85** (2012) 056011, [arXiv:1109.4398].

[27] CMS Collaboration: S. Chatrchyan *et. al.*, *Search for Dark Matter and Large Extra Dimensions in pp Collisions Yielding a Photon and Missing Transverse Energy*, *Phys. Rev. Lett.* **108** (2012) 261803, [arXiv:1204.0821].

[28] ATLAS Collaboration: G. Aad *et. al.*, *Search for dark matter in events with a Z boson and missing transverse momentum in pp collisions at* $\sqrt{s}$*=8 TeV with the ATLAS detector*, *Phys. Rev. D* **90** (2014) 012004, [arXiv:1404.0051].

[29] Fermi-LAT Collaboration: M. Ackermann *et. al.*, *Dark Matter Constraints from Observations of 25 Milky Way Satellite Galaxies with the Fermi Large Area Telescope*, *Phys. Rev. D* **89** (2014) 042001, [arXiv:1310.0828].

[30] T. Daylan, D. P. Finkbeiner, *et. al.*, *The Characterization of the Gamma-Ray Signal from the Central Milky Way: A Compelling Case for Annihilating Dark Matter*, arXiv:1402.6703.

[31] H.E.S.S. Collaboration: A. Abramowski *et. al.*, *H.E.S.S. constraints on Dark Matter annihilations towards the Sculptor and Carina Dwarf Galaxies*, *Astropart. Phys.* **34** (2011) 608–616, [arXiv:1012.5602].

[32] MAGIC Collaboration: J. Aleksi, S. Ansoldi, *et. al.*, *Optimized dark matter searches in deep observations of Segue 1 with MAGIC*, *JCAP* **02** (2014) 008, [arXiv:1312.1535].

[33] VERITAS Collaboration: A. Geringer-Sameth, *The VERITAS Dark Matter Program*, arXiv:1303.1406.

[34] H.E.S.S. Collaboration: A. Abramowski *et. al.*, *Search for a Dark Matter annihilation signal from the Galactic Center halo with H.E.S.S*, *Phys. Rev. Lett.* **106** (2011) 161301, [arXiv:1103.3266].

[35] CTA Consortium: M. Actis *et. al.*, *Design concepts for the Cherenkov Telescope Array CTA: An advanced facility for ground-based high-energy gamma-ray astronomy*, *Exper. Astron.* **32** (2011) 193–316, [arXiv:1008.3703].

[36] CTA Consortium: M. Doro *et. al.*, *Dark Matter and Fundamental Physics with the Cherenkov Telescope Array*, *Astropart. Phys.* **43** (2013) 189–214, [arXiv:1208.5356].

[37] M. Wood, J. Buckley, *et. al.*, *Prospects for Indirect Detection of Dark Matter with CTA*, arXiv:1305.0302.

[38] M. Pierre, J. M. Siegal-Gaskins, and P. Scott, *Sensitivity of CTA to dark matter signals from the Galactic Center*, *JCAP* **6** (2014) 24, [arXiv:1401.7330].

[39] H.E.S.S. Collaboration: F. Aharonian *et. al.*, *Observations of the Crab Nebula with H.E.S.S*, *A&A* **457** (2006) 899–915, [astro-ph/0607333].

[40] VERITAS Collaboration: J. Holder *et. al.*, *The first VERITAS telescope*, *Astropart. Phys.* **25** (2006) 391–401, [astro-ph/0604119].

[41] K. Bernlöhr, A. Barnacka, *et. al.*, *Monte Carlo design studies for the Cherenkov Telescope Array*, *Astropart. Phys.* **43** (2013) 171–188, [arXiv:1210.3503].

[42] A. M. Hillas, *Cerenkov light images of EAS produced by primary gamma*, *International Cosmic Ray Conference* **3** (1985) 445–448.

[43] J. G. Skellam, *The frequency distribution of the difference between two poisson variates belonging to different populations*, *J. Royal Stat. Soc.* **109** (1946) 296.

[44] J. M. Cline, K. Kainulainen, P. Scott, and C. Weniger, *Update on scalar singlet dark matter*, *Phys. Rev. D* **88** (2013) 055025, [arXiv:1306.4710].

[45] Fermi-LAT Collaboration: M. Ackermann *et. al.*, *The Fermi Large Area Telescope On Orbit: Event Classification, Instrument Response Functions, and Calibration*, *ApJS* **203** (2012) 4, [arXiv:1206.1896].

[46] J. F. Navarro, E. Hayashi, *et. al.*, *The inner structure of ΛCDM haloes - III. Universality and asymptotic slopes*, *MNRAS* **349** (2004) 1039–1051, [astro-ph/0311231].

[47] L. Pieri, J. Lavalle, G. Bertone, and E. Branchini, *Implications of High-Resolution Simulations on Indirect Dark Matter Searches*, *Phys.Rev.* **D83** (2011) 023518, [arXiv:0908.0195].

[48] M. Cirelli, G. Corcella, *et. al.*, *PPPC 4 DM ID: A Poor Particle Physicist Cookbook for Dark Matter Indirect Detection*, *JCAP* **1103** (2011) 051, [arXiv:1012.4515].

[49] Fermi LAT Collaboration: A. A. Abdo *et. al.*, *Measurement of the Cosmic Ray e+ plus e- spectrum from 20 GeV to 1 TeV with the Fermi Large Area Telescope*, *Phys. Rev. Lett.* **102** (2009) 181101, [arXiv:0905.0025].

[50] H.E.S.S. Collaboration: F. Aharonian *et. al.*, *The energy spectrum of cosmic-ray electrons at TeV energies*, *Phys. Rev. Lett.* **101** (2008) 261104, [arXiv:0811.3894].

[51] J. R. Hoerandel, *On the knee in the energy spectrum of cosmic rays*, *Astropart. Phys.* **19** (2003) 193–220, [astro-ph/0210453].

[52] D. Fegan, *Gamma/hadron separation at TeV energies*, *J. Phys. G* **23** (1997) 1013–1060.

[53] H.E.S.S. Collaboration: F. Aharonian *et. al.*, *Discovery of Very-High-Energy Gamma-Rays from the Galactic Centre Ridge*, *Nature* **439** (2006) 695–698, [astro-ph/0603021].

[54] Fermi-LAT Collaboration: M. Ackermann *et. al.*, *Fermi-lat observations of the diffuse gamma-ray emission: Implications for cosmic rays and the interstellar medium*, *ApJ* **750** (2012) 3, [arXiv:1202.4039].

[55] S. Funk and J. A. Hinton, *Comparison of Fermi-LAT and CTA in the region between 10-100 GeV*, *Astropart. Phys.* **43** (2013) 348–355, [arXiv:1205.0832].

[56] H. Dickinson and J. Conrad, *Handling Systematic Uncertainties and Combined Source Analyses for Atmospheric Cherenkov Telescopes*, *Astropart.Phys.* **41** (2013) 17–30, [arXiv:1203.5643].

[57] G. Cowan, K. Cranmer, E. Gross, and O. Vitells, *Asymptotic formulae for likelihood-based tests of new physics*, *Eur. Phys. J. C* **71** (2011) 1554, [arXiv:1007.1727].

[58] G. J. Feldman and R. D. Cousins, *A Unified approach to the classical statistical analysis of small signals*, *Phys.Rev.* **D57** (1998) 3873–3889, [physics/9711021].

[59] I. Cholis and P. Salucci, *Extracting limits on Dark Matter annihilation from gamma-ray observations towards dwarf spheroidal galaxies*, *Phys.Rev.* **D86** (2012) 023528, [arXiv:1203.2954].

[60] L. Bergstrom, G. Bertone, J. Conrad, C. Farnier, and C. Weniger, *Investigating Gamma-Ray Lines from Dark Matter with Future Observatories*, *JCAP* **1211** (2012) 025, [arXiv:1207.6773].

[61] H.E.S.S. Collaboration: A. Abramowski *et. al.*, *Search for photon line-like signatures from Dark Matter annihilations with H.E.S.S*, *Phys.Rev.Lett.* **110** (2013) 041301, [arXiv:1301.1173].